AAS 24-063

LEVERAGING RESONANT TERMINATOR ORBITS FOR THE TRAJECTORY DESIGN OF OSIRIS-APEX AT (99942) APOPHIS

Gavin M. Brown[*], Daniel R. Wibben[*], Peter G. Antreasian[*], and Kenneth M. Getzandanner[†]

The OSIRIS-REx spacecraft has been approved for an extended mission (OSIRIS-APEX) to visit the asteroid (99942) Apophis. In this paper we outline a potential design for the spacecraft's trajectory during the variable phase orbit segment of the APEX mission. This phase of the mission, nominally expected to begin in January 2030, has the primary goal of collecting image and spectral data of the full asteroid surface at a wide variety of illumination conditions without requiring frequent firing of the spacecraft thrusters. This work will focus on leveraging resonant terminator orbits (RTOs) in order to satisfy these goals and the associated science requirements. Though this segment will occur after Apophis' closest flyby of Earth in April 2029, the proposed design utilizes the current best estimates of the asteroid's orbital elements and physical properties at that time when designing the spacecraft's orbit.

INTRODUCTION

The terminator orbit family is a desirable family of periodic orbits as a number of the orbits are stable when considering large solar radition pressure (SRP).[1] In the stable region of this family, there are numerous period multiplying bifurcations that occur, which give rise to a set of new periodic orbit families whose members are referred to as resonant terminator orbits (RTOs).[1,2] The general structure of the RTO families have been studied previously.[1] These RTOs are of practical interest as the extended OSIRIS-REx mission,[3] which is referred to as OSIRIS-APEX, currently plans to use an orbit similar to a RTO during the Variable Phase Orbit segment of its mission at the asteroid (99942) Apophis.[4]

Several important parameters needed to define the dynamical environment around Apophis are currently unknown. For example, the spin state of the asteroid during the VPO segment is unknown as the asteroid will have a close encounter with Earth in April of 2029.[4–6] Several of the orbital elements describing Apophis' orbit about the Sun will change after the encounter as well. In addition, the current estimate for the gravitational parameter of Apophis ranges from 1.36 to 4.37 m^3/s^2.[4] With that in mind, we seek to develop a toolkit that can generate a trajectory with desirable characteristics for the VPO segment of the APEX mission considering the large range of possible model parameter values. We will begin by discussing the computation of RTOs in the vicinity of Apophis using an idealized model which approximates the asteroid as a point mass in a circular orbit around the Sun. We will then discuss how we correct the initial trajectory using a more realistic model that accounts for the eccentricity of the asteroid's orbit and uses a higher fidelity representation of its gravitational attraction. Will then present the trajectories obtained from the toolkit over a range of possible values of the gravitational parameter of Apophis.

[*]KinetX, Inc. Space Navigation and Flight Dynamics Practice, 21 W. Easy St., Ste 108, Simi Valley, CA 93065, USA.

[†]NASA/GSFC Code 595, 8800 Greenbelt Rd, Greenbelt, MD 20771, USA.

RESONANT TERMINATOR ORBITS

Augmented Normalized Hill 3-Body Problem Model

The Augmented Normalized Hill 3-Body Problem (ANH3BP) model is a dynamical model accounting for the gravitational effect of the Sun and a primitive body, as well as SRP, on a spacecraft.[1,7] When the orbit of the primitive body and the Sun is circular, the Jacobi constant is a conserved quantity and the system is autonomous.[7] The equations of motion for the ANH3BP will now be presented based on Section 2 of Ref. 7.

Let μ_S represent the gravitational parameter of the Sun, and let p_S, e_S, and f represent the orbit parameter, eccentricity, and true anomaly of the primitive body's orbit around the Sun. The position vector of the primitive body relative to the Sun is represented by $\boldsymbol{d} = d\hat{\boldsymbol{d}}$ and the angular velocity vector of the primitive body's orbit around the Sun is represented by $\boldsymbol{\Omega} = \Omega\hat{\boldsymbol{\Omega}}$ where $\Omega = \dot{f}$ and $\hat{\boldsymbol{\Omega}}$ is the fixed direction perpendicular to the plane of that orbit. In this work, $\dot{a}$ will represent the time derivative of the quantity a and a' will represent the derivative of the quantity a with respect to f (i.e., $\dot{a} = \frac{\mathrm{d}a}{\mathrm{d}t}$ and $a' = \frac{\mathrm{d}a}{\mathrm{d}f}$). We will define a coordinate frame $\mathcal{A} : \{\hat{\boldsymbol{x}}, \hat{\boldsymbol{y}}, \hat{\boldsymbol{z}}\}$ with an origin at the center of mass of the primitive body such that $\hat{\boldsymbol{x}} = \hat{\boldsymbol{d}}$ and $\hat{\boldsymbol{z}} = \hat{\boldsymbol{\Omega}}$. Units of distance will be scaled such that 1 DU $= d\epsilon$ where $\epsilon = (\mu/\mu_S)^{1/3}$ and μ is the gravitational parameter of the primitive body. Expressions for these quantities are provided in the following equations.[7]

$$d = \frac{p_S}{1 + e_S \cos f} \tag{1a}$$

$$\Omega = \frac{\sqrt{\mu_S p_S}}{d^2} \tag{1b}$$

$$d' = \frac{d^2}{p_S} e_S \sin f \tag{1c}$$

$$\dot{\Omega} = -2\sqrt{\frac{\mu_S}{p_S}} \frac{e_S \sin f \Omega}{d} \tag{1d}$$

Let $\boldsymbol{r}$ represent the position vector of a spacecraft of negligible mass in the vicinity of the primitive body whose components are represented in the $\mathcal{A}$-frame in scaled units of DU. In the"pulsating frame", the equations of motion are:

$$\boldsymbol{r}'' = -2\hat{\boldsymbol{\Omega}} \times \boldsymbol{r}' - \hat{\boldsymbol{\Omega}} \cdot \boldsymbol{r} + \boldsymbol{g} + \frac{1}{1 + e_S \cos f} \left(\tilde{\beta} + 3x\right) \hat{\boldsymbol{x}} \tag{2a}$$

$$\tilde{\beta} = \frac{G_1}{B\mu_S \epsilon} \tag{2b}$$

$$\boldsymbol{g}_{\text{pm}} = -\frac{1}{1 + e_S \cos f} \frac{1}{r^3} \boldsymbol{r} \tag{2c}$$

where $\boldsymbol{g}$ is the gravitational attraction of the primitive body, $G_1 = 1 \times 10^8$ kg km^3/s^2/m^2, and B is the spacecraft mass to area ratio.[7,8] Note that the gravitational attraction when the primitive body is approximated as a point mass (i.e., $\boldsymbol{g} = \boldsymbol{g}_{\text{pm}}$) is given in Eq. (2c). The following expressions can be used to convert to dimensional quantities.[7]

$$\boldsymbol{R} = \epsilon d \boldsymbol{r} \tag{3a}$$

$$\dot{\boldsymbol{R}} = \epsilon\Omega \left(d'\boldsymbol{r} + d\boldsymbol{r}'\right) \tag{3b}$$

It is important to note that the Variable Phase Orbit (VPO) segment of the mission to Apophis is currently planned to start after Apophis' flyby of Earth in 2029.[4] As a result, the orbital elements of Apophis' orbit around the Sun, as well as its spin state, have large uncertainties. Also, several important physical characteristics of the asteroid, such as the gravitational parameter, have large uncertainties as well. Table 1 and Table 2 contain the parameters used in this work, although it should be noted that many of these values could change as better estimates are obtained.

Table 1 Estimates of the Orbit Parameters of Apophis Post-Encounter.

Orbit Parameters[4,9]	
Semi-major axis, a_{S} (m)	$1.650227501552187 \times 10^{11}$
Eccentricity, e_{S}	0.1890650444165436
Inclination, i (deg)	2.221099203220031
Longitude of ascending node, Ω_{S} (deg)	203.5628891952976
Argument of perifocus, ω_{S} (deg)	71.43287204673284
Time of periapsis, τ_{S} (Julian Day)	2462301.148680804763
Epoch	Jun. 1, 2029

Table 2 Estimates of the Rotation and Physical Parameters of Apophis Post-Encounter.

Rotation Parameters		**Physical and Other Parameters**	
Precession angle, ϕ (deg)	0	Gravitational Parameter, μ ($\mathrm{m}^3/\mathrm{s}^2$)[4]	2.68 (1.36-4.37)
Nutation angle, θ (deg)[10]	37	Mass-to-projected area, B (kg/m^2)	81.119
Rotation angle, ψ (deg)	0	Start Date[4]	Jan. 15, 2030
Precession period, T_ϕ (hr)[10,11]	27.38	End Date[4]	Apr. 1, 2030
Rotation period, T_ψ (hr)[10,12]	266		
β_L (deg)[10]	250		
λ_L (deg)[10]	-75		

We will only consider variations in μ as that directly affects the scaling of the SRP as can be seen in Eq. (2b). We considered the minimum, best, and maximum estimates of μ in this work, which are $\mu_{\mathrm{min}} = 1.36$, $\mu_{\mathrm{cbe}} = 2.68$, and $\mu_{\mathrm{max}} = 4.37$ $\mathrm{m}^3/\mathrm{s}^2$, respectively. Note that the rotation parameters shown in Table 2 are not incorporated unless the polyhedron gravity model is used. An initial value of zero was assigned to ϕ and ψ, although this should be updated when better estimates are known. While θ will be time-varying, for the preliminary implementation of this model used for these simulations it was set to be a fixed mean value estimated in Ref. 10. The start and end dates were set based on the planned VPO mission segment presented in Figure 13 of Ref. 4.

Periodic Orbit Families in the Circular ANH3BP

When the eccentricity of a primitive body's orbit about the Sun is zero d and Ω are constant, and the system described by Eq. (2) (when using $\boldsymbol{g} = \boldsymbol{g}_{\mathrm{pm}}$) is autonomous. In this system periodic orbits exist in continuous one parameter families. Equilibrium points may also be identified, including the "dark-side" equilibrium point which lies on the $+x$-axis. This point may be computed by identifying

the value of $x > 0$ where $\boldsymbol{r} = [x\,0\,0]^T$ and $\boldsymbol{r}' = \boldsymbol{0}$ such that $\boldsymbol{r}'' = \boldsymbol{0}$ in Eq. (2a). A planar family can be computed by analyzing the linearized system evaluated at this point. By continuing this planar family, a bifurcation occurs where a new periodic orbit family can be identified that rises out of the plane. Continuing this family produces a set of periodic orbits which are known as terminator orbits. In the stable region of the terminator orbit family, there are many period-multiplying bifurcations where additional families can be computed starting at those points. The orbits in these families are referred to as resonant terminator orbits. We used a variable step-size pseudo-arclength continuation scheme to compute these families.

Several of these RTO families have been computed previously.[1,2] In Ref. 1, Broschart et al. outline the two primary types of these RTOs: Sun-side and dark-side. The Sun-side RTOs are of interest as they possess desirable characteristics for observations and measurement of the primitive body. For this reason, we computed the dark-side equilibrium point, planar family, terminator orbit family, and many of the Sun-side RTO families at the three different values of μ discussed previously. To distinguish between the different RTO families, each will be given an identifier $m\mathrm{T}n$ where m corresponds to the specific bifurcation (e.g., $m = 2$ and $m = 3$ correspond to a period-doubling and period-tripling bifurcation, respectively) and n corresponds to order of that particular bifurcation (e.g., 3T4 corresponds to the Sun-side RTO family found at the fourth period-tripling bifurcation point on the terminator orbit). We attempted to compute these families starting at the appropriate bifurcation points with values of $1 \leq m \leq 10$. We computed the families in the direction such that that the initial states were of the form $\boldsymbol{X}_0 = [x\,0\,z\,0\,\dot{y}\,0]^T$ where $z \geq 0$. Using $\mu = \mu_{\text{cbe}}$, the terminator orbits corresponding to the bifurcation points are shown in Figure 1, as are several orbit members of the 5T6 RTO family.

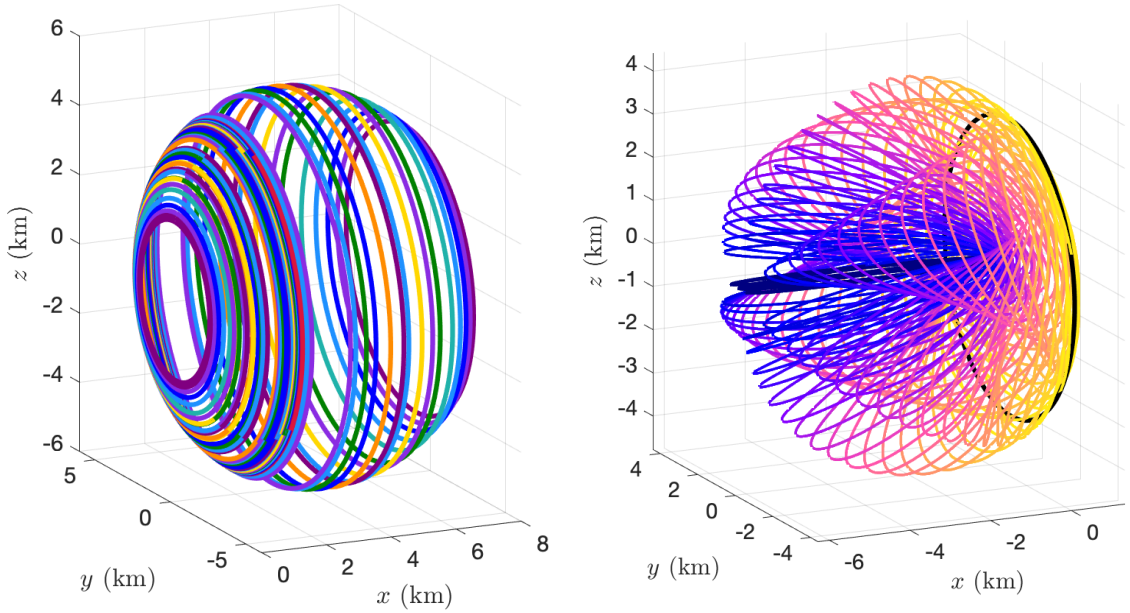

Figure 1 Circular ANH3BP Orbit Families. Left: terminator orbits corresponding to period-multiplying bifurcation points with $m = 1$ to 10 shown in red to purple. Right: members of the Sun-side 5T6 RTO family starting from the terminator orbit shown in black, where each color represents a different orbit member.

The most important characteristics of an RTO to consider for the VPO segment are the minimum

phase angle ϕ_{min}, periapsis distance R_p, and apoapsis distance R_a.[4] Preliminary estimates of the desired values of the VPO are $R_p = 1$ km, $R_a = 4.5$ km, and $\phi_{\text{min}} = 45$ deg. The rotation of the orbit plane with each pass of the asteroid is related to the value of m. To convert the distances to dimensional units for these RTOs, we treated the initial orbit of Apophis as a circular orbit with a semi-major axis of a_S. Plots depicting the relationship between ϕ_{min} and r_p for each of the RTO families identified (the 3T3, 4T3, 5T6, 6T3, 7T9, and 8T7 RTO families) are presented in Figure 2. As can be seen in this figure, RTOs in families with smaller values of m have larger closest approach distances at the same minimum phase angle compared to RTOs in families with larger values of m. Similarly, an orbit with a specific minimum phase angle in a particular mTn RTO family will have a larger closest approach distance at larger values of μ.

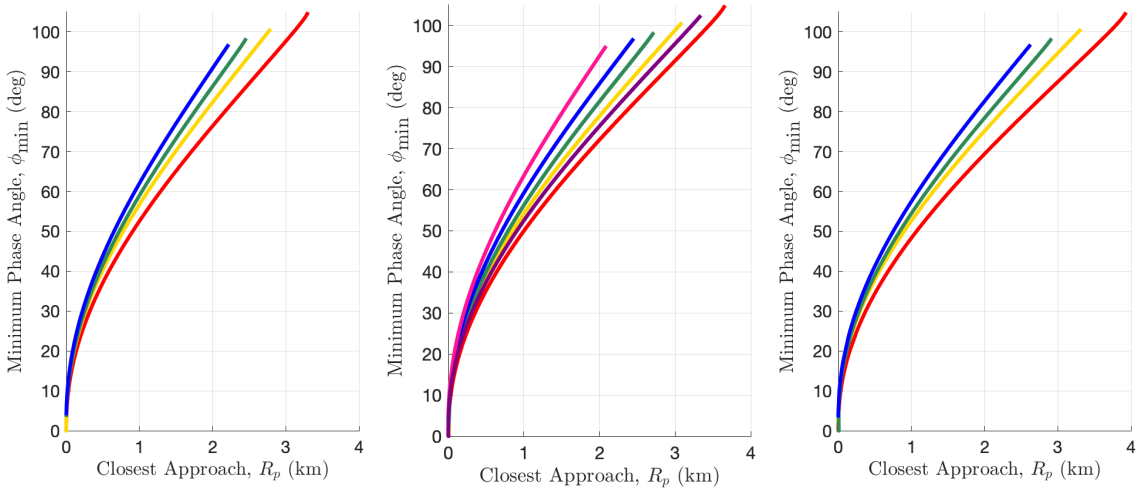

Figure 2 Circular ANH3BP RTO Characteristics for μ_{min} (left), μ_{cbe} (middle), μ_{max} (right). The 3T3, 4T3, 5T6, 6T3, 7T9, and 8T7 RTO families are represented by the red, yellow, green, blue, purple, and pink lines, respectively.

CORRECTIONS PROCEDURE

Realistic Considerations

While the circular ANH3BP is useful for obtaining the initial representation of an RTO that can be used in the VPO segment, there are additional effects that must be incorporated into the model to obtain a more realistic orbit. The two primary adjustments we will make the model involve the non-zero eccentricity of Apophis' orbit and using a higher-fidelity model to represent the gravitational effect of Apophis compared to the point-mass model used in the circular ANH3BP. For each RTO family, we selected the member with ϕ_{min} closest to a value of 50 deg, which is close to the value of 45 deg specified in Ref. 4.

Accounting for non-zero eccentricity introduces an explicit dependence on f (i.e., time) to the equations of motion in Eq. (2a). As a result, the initial time of the VPO segment, which was not necessary for the model with a circular orbit, must now be accounted for in the model. Furthermore, as f is used as the "time", we integrate the equations of motion and then convert back to true time

using Kepler's equation.

$$E = 2\arctan\left(\frac{\sqrt{1-e}}{\sqrt{1+e}}\tan\left(\frac{f}{2}\right)\right) \tag{4a}$$

$$n = \sqrt{\frac{\mu}{a_{\mathrm{S}}^3}} \tag{4b}$$

$$M = n\left(t-\tau\right) \tag{4c}$$

Using a more realistic representation of the gravity field around Apophis introduces another time-dependent term in the equations. The shape model of Apophis we use in this study has 3996 faces.[4,11] We use a constant-density polyhedron model to represent the gravity field of the asteroid. The form of the gravitational attraction when using this model is given in Eq. (5).[8]

$$\boldsymbol{g}_{\mathrm{ph}} = \frac{1}{\epsilon d\Omega^2}\left[AB\right]\left(-G\sigma\sum_{e=1}^{n_e}\boldsymbol{E}_e \bullet \boldsymbol{r}_e \cdot L_e + G\sigma\sum_{f=1}^{n_f}\boldsymbol{F}_f \bullet \boldsymbol{r}_f \cdot \omega_f\right) \tag{5a}$$

Please refer to Ref. 8 for a detailed discussion of the terms in Eq. (5a). Note that the dimensional position vector $\boldsymbol{R}$ should be used in the computations. Also note that the mass distribution of the asteroid is not constant in the $\mathcal{A}$-frame, so the relevant transformation matrices must be used. Let the $\mathcal{B}$-frame be defined as the frame with an origin at the center of the primitive body where the mass distribution remains constant. Then the rotation matrix $[AB]$ can be obtained by using Eq. 20 in the Appendix of Ref. 10 as well as an additional rotation from the ecliptic frame to the $\mathcal{A}$-frame based on the orbital elements of the primitive body.

Correcting the Orbit

Before attempting to obtain a corrected orbit with these additional effects, a preliminary calculation was performed to adjust the velocity and "period" of the initial RTO obtained in the circular ANH3BP. Based on the form of the equations of motion, the "period" used in our calculations is the change in true anomaly Δf over the period of the orbit. In this preliminary analysis the value of $\dot{y}$ for the initial orbit was multiplied by different scaling factors (we used 100 values normally in the range of 0.85-1.15). Each of these new states was integrated up to $1.5\Delta f$ where Δf corresponds to the "period" of the initial orbit. The point on each of these trajectories closest to the initial state was identified and the distance between each of these points and the initial state was computed. The trajectory with the minimum distance was selected as the updated initial guess for use in a differential corrections scheme.

The differential corrector allowed the initial velocity and Δf to match the final position with the initial position. If the resulting Δf was less than the change in true anomaly corresponding to the end date of the VPO segment in Table 2, this corrections process was repeated to generate additional orbit cycles until the final time was past Apr. 1, 2030. While position continuity was always enforced, an impulsive burn was allowed to occur after each completed orbit cycle.

RESULTS

The orbits identified using $\mu = \mu_{\mathrm{cbe}}$ were computed first. Each of the corrected trajectories consisted of two orbit cycles. The final trajectories are shown in Figure 3. The characteristics of

these orbits are presented in Table 3, including the burn magnitudes, total propagation time for the trajectories shown in Figure 3, as well as the time for the spacecraft to depart the vicinity of the asteroid starting with the initial guess and corrected initial state if no burns were allowed to occur.

Table 3 Characteristics of the Corrected Trajectories Resulting from RTOs with $\mu = \mu_{\text{cbe}}$.

Result from Initial RTO Family	3T3	4T3	5T6	6T3	7T9	8T7
Closest Distance, R_{min} (km)	0.71	0.48	0.61	0.41	0.64	0.26
Farthest Distance, R_{max} (km)	4.89	4.41	3.92	3.53	4.43	2.95
Minimum Phase Angle, ϕ_{min} (deg)	47.37	45.55	47.89	43.75	45.73	40.88
Burn 1, ΔV_1 (mm/s)	7.07	9.83	3.62	8.69	8.63	4.35
Total Period, T_F (days)	72.40	78.78	84.04	85.34	132.74	89.24
Ejection Time - No Burns, T_E (days)	99.77	132.36	181.80	> 674.15	140.57	196.32

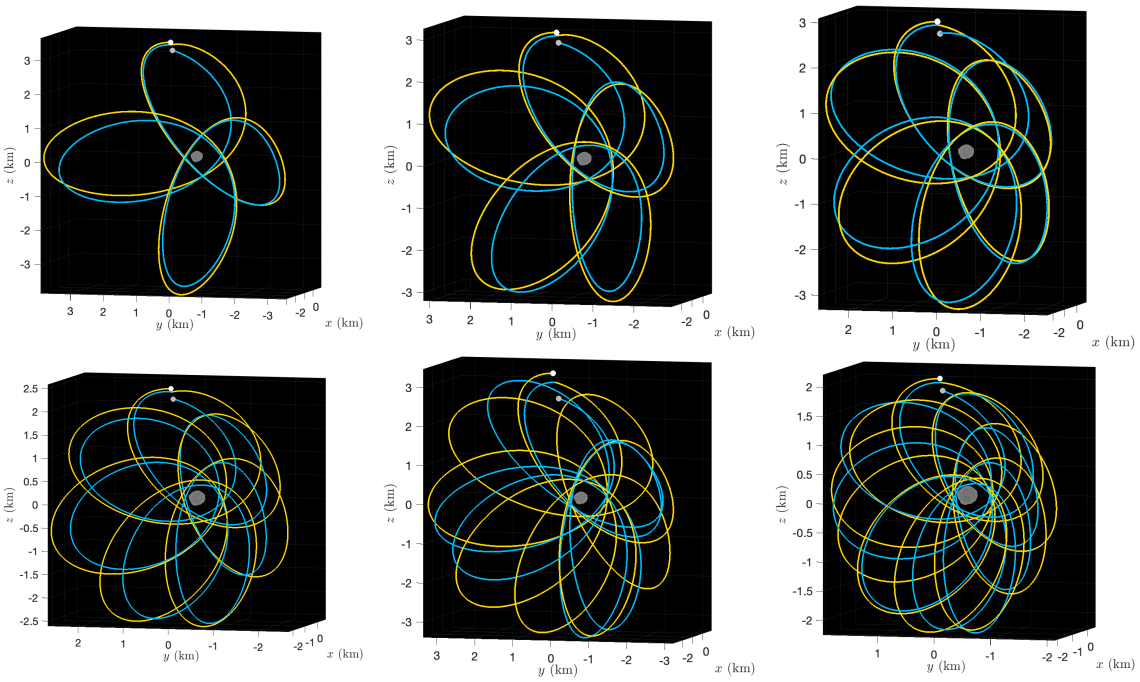

Figure 3 Corrected Trajectories Resulting from RTOs with $\mu = \mu_{\text{cbe}}$. From left to right then top down: 3T3, 4T3, 5T6, 6T3, 7T9, and 8T7. The first cycle is shown in yellow and the second is shown in light blue.

The current start date is set at Jan. 15, 2030, which is when Apophis is nearly at the apoapsis of its orbit about the Sun.[4] However, in the case that the start date is delayed, it is important that the planned orbits can still be corrected when Apophis is closer to its periapsis. While all of these orbits were successfully corrected, the orbits corresponding to the 3T3 and 4T3 families demonstrate the most promise in this regard, as these orbits were the easiest to correct. It is also important to note that as the scaling of distance quantities varies with the orbit of Apophis around the Sun, the variations in the distance of the spacecraft from Apophis and the phase angle of the corrected orbit from the 3T3 family are shown in Figure 4.

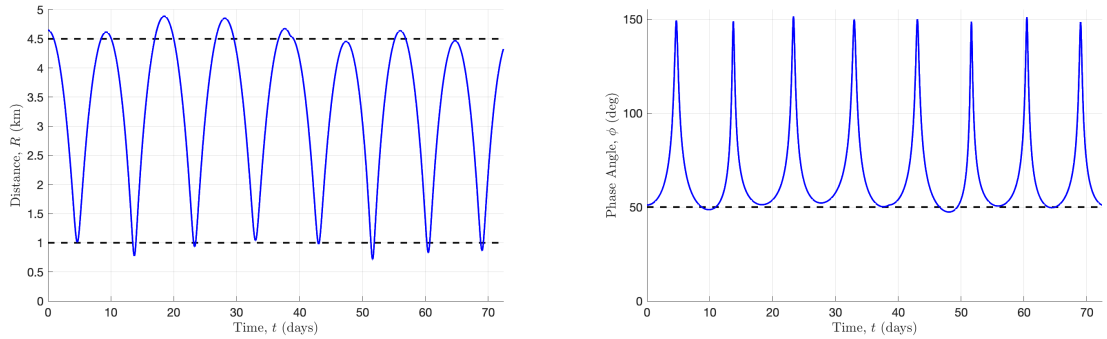

Figure 4 Characteristics of the Corrected Trajectory Resulting from the 3T3 RTO Family with $\mu = \mu_{\text{cbe}}$. The black dashed lines represent values of $R = 1$ km and $R = 4.5$ km (left) and $\phi = 45$ deg (right).

The result using the orbit from the 6T3 family was also interesting. When propagating the corrected initial state for this orbit in the more realistic model, and not allowing impulsive burns, the spacecraft did not depart the vicinity of the asteroid for at least 674.15 days. This was the longest departure time of any of the orbits tested. Figure 5 shows the long duration integrated trajectories with no burns allowed. The trajectories were integrated until the spacecraft departed the vicinity of the asteroid (i.e., $r \geq 10$ DU) or the specified maximum integration time of 674.15 days was reached.

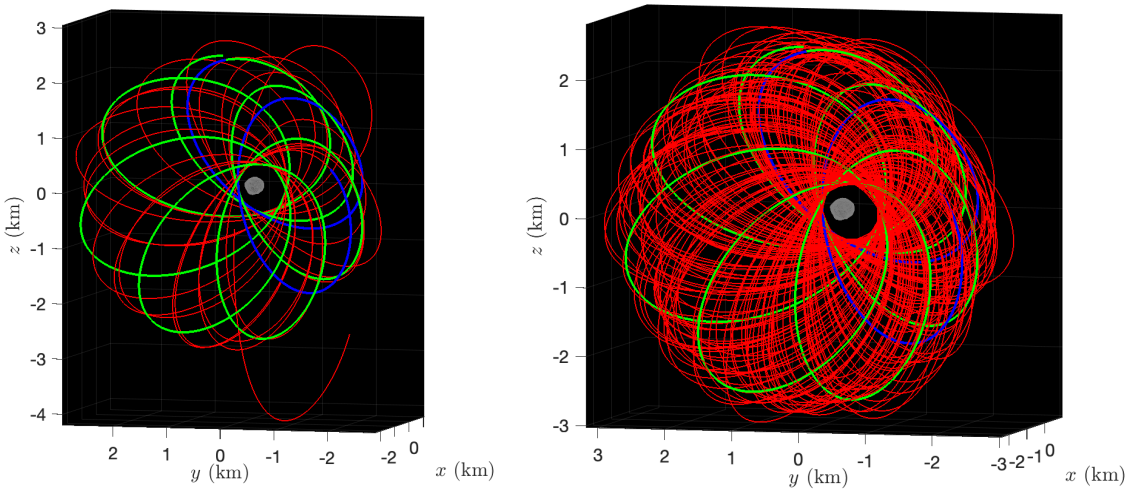

Figure 5 Ejection Time of Corrected Orbit from RTO 6T3 with $\mu = \mu_{\text{CBE}}$. Initial Condition from the Initial Guess (left) and Corrected Orbit (right). Green is the portion of the trajectory up to the end of the first cycle, blue is the portion of the trajectory up to the duration of the VPO segment duration, and red is the portion of the trajectory up to the time of departure or the maximum integration time was reached.

Corrected Orbits for Other Possible Values of μ

Using $\mu = \mu_{\text{min}}$, the parameters of the corrections procedure required more manual adjustment to achieve convergence. It was more difficult to correct the trajectories for this value of μ. For

this reason we only focused on corrections for the 3T3, 4T3, and 5T6 RTO families. Each of the corrected trajectories consisted of three orbit cycles. The characteristics of these corrected orbits are presented in Table 4, and the corresponding trajectories are shown in Figure 6.

Table 4 Characteristics of the Corrected Trajectories Resulting from RTOs with $\mu = \mu_{\text{min}}$.

Result from Initial RTO Family	3T3	4T3	5T6
Closest Distance, R_{min} (km)	0.50	0.41	0.23
Farthest Distance, R_{max} (km)	3.57	3.08	2.98
Minimum Phase Angle, ϕ_{min} (deg)	44.86	43.09	34.63
Burn 1, ΔV_1 (mm/s)	1.32	4.63	3.40
Burn 2, ΔV_2 (mm/s)	1.77	6.05	8.20
Total Period, T_F (days)	88.96	96.79	101.79
Ejection Time - No Burns, T_E (days)	88.90	154.79	251.94

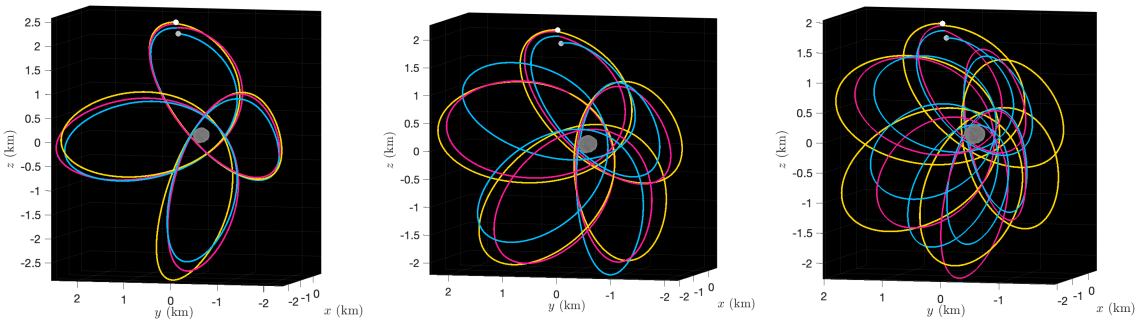

Figure 6 Corrected Trajectories Resulting from RTOs with $\mu = \mu_{\text{min}}$. From left to right then top down: 3T3, 4T3, and 5T6. The first cycle is shown in yellow, the second is shown in pink, and the third is shown in light blue.

Using $\mu = \mu_{\text{max}}$it was significantly easier to correct the trajectories. With this value of μ we focused on the 3T3, 4T3, 5T6, and 6T3 RTO families. Each of the corrected trajectories consisted of two orbit cycles. The characteristics of these corrected orbits are presented in Table 5, and the corresponding trajectories are shown in Figure 7.

Table 5 Characteristics of the Corrected Trajectories Resulting from RTOs with $\mu = \mu_{\text{max}}$.

Result from Initial RTO Family	3T3	4T3	5T6	6T3
Closest Distance, R_{min} (km)	0.91	0.59	0.54	0.66
Farthest Distance, R_{max} (km)	6.16	5.35	4.98	4.46
Minimum Phase Angle, ϕ_{min} (deg)	45.34	41.86	42.38	46.90
Burn 1, ΔV_1 (mm/s)	6.12	5.13	5.34	7.03
Total Period, T_F (days)	81.73	84.35	88.54	96.10
Ejection Time - No Burns, T_E (days)	116.71	155.23	180.10	201.39

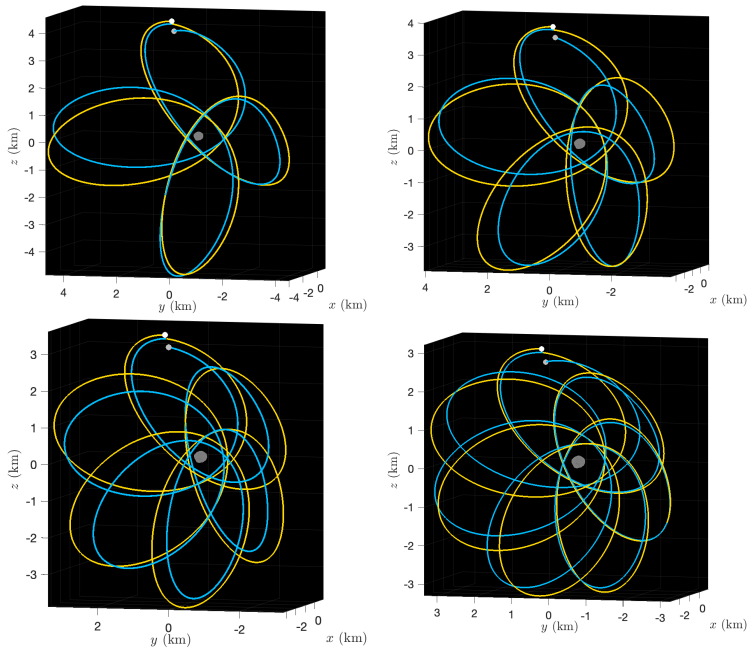

Figure 7 Corrected Trajectories Resulting from the RTOs with $\mu = \mu_{\max}$. From left to right then top down: 3T3, 4T3, 5T6, and 6T3. The first cycle is shown in yellow and the second is shown in light blue.

CONCLUSION

There is great potential to leverage the structures of Resonant Terminator Orbits (RTOs) for the Variable Phase Orbit (VPO) phase of the OSIRIS-APEX mission to the asteroid Apophis. We were able to identify several candidate orbits that persisted in a more realistic model of the dynamics that accounted for the shape and complex rotation of the asteroid, as well as the eccentricity of Apophis' orbit about the Sun. While further analysis and modification will be needed to consider additional effects, this work indicates that over the range of posible parameters associated with the orbit and physical properties of Apophis, these RTOs can serve as a useful reference point for generating the trajectory to be used during the VPO phase.

ACKNOWLEDGMENT

This material is based upon work supported by NASA under Contracts NNM10AA11C and NNG13FC02C. OSIRIS-APEX is the extended mission of OSIRIS-REx, the third mission in NASA's New Frontiers Program. Daniella DellaGiustina of the University of Arizona, Tucson, is the mission's Principal Investigator, and the University of Arizona also leads the Science Team and the science observation planning and data processing. Lockheed Martin Space Systems in Denver built the spacecraft and is providing flight operations. Goddard Space Flight Center and KinetX Aerospace are responsible for navigating the OSIRIS-REx spacecraft. Contract NNM10AA11C is issued through the New Frontiers Program.

REFERENCES

[1] S. B. Broschart, G. Lantoine, and D. J. Grebow, "Quasi-terminator orbits near primitive bodies," *Celestial Mechanics and Dynamical Astronomy*, Vol. 120, Aug 2014, pp. 195–215.

[2] S. B. Broschart, D. J. Scheeres, and B. F. Villac, "New Families of Multi-Revolution Terminator Orbits near Small Bodies," *AAS/AIAA Astrodynamics Specialist Conference*, Aug 2009.
[3] D. S. Lauretta, S. S. Balram-Knutson, E. Beshore, *et al.*, "OSIRIS-REx: Sample Return from Asteroid (101955) Bennu," *Space Science Reviews*, Vol. 212, Aug 2017, p. 925–984.
[4] D. N. DellaGiustina, M. C. Nolan, A. T. Polit, *et al.*, "OSIRIS-APEX: An OSIRIS-REx Extended Mission to Asteroid Apophis," *The Planetary Science Journal*, Vol. 4, Oct 2023.
[5] D. J. Scheeres, S. J. Ostro, R. A. Werner, E. Asphaug, and R. S. Hudson, "Effects of Gravitational Interactions on Asteroid Spin States," *Icarus*, Vol. 147, Sep 2000, pp. 106–118.
[6] D. C. Richardson, W. F. Bottke, and S. G. Love, "Tidal Distortion and Disruption of Earth-Crossing Asteroids," *Icarus*, Vol. 134, Jul 1998, pp. 47–76.
[7] D. J. Scheeres and F. Marzari, "Spacecraft Dynamics in the Vicinity of a Comet," *The Journal of the Astronautical Sciences*, Vol. 50, Mar 2002, pp. 35–52.
[8] R. A. Werner and D. J. Scheeres, "Exterior gravitation of a polyhedron derived and compared with harmonic and mascon gravitation representations of asteroid 4769 Castalia," *Celestial Mechanics and Dynamical Astronomy*, Vol. 65, Sep 1996, pp. 313–344.
[9] NASA Jet Propulsion Laboratory Solar System Dynamics Group, "JPL Horizons on-line ephemeris system," `https://ssd.jpl.nasa.gov/horizons/app.html#/`, 2022. Online; accessed 02 July 2023.
[10] P. Pravec, P. Scheirich, J. Ďurech, *et al.*, "The tumbling spin state of (99942) Apophis," *Icarus*, Vol. 233, May 2014, pp. 48–60.
[11] M. Brozović, L. A. Benner, J. G. McMichael, *et al.*, "Goldstone and Arecibo radar observations of (99942) Apophis in 2012–2013," *Icarus*, Vol. 300, 2018, pp. 115–128.
[12] C. J. Benson, D. J. Scheeres, M. Brozović, S. R. Chesley, P. Pravec, and P. Scheirich, "Spin state evolution of (99942) Apophis during its 2029 Earth encounter," *Icarus*, Vol. 390, 2023, p. 115324.